

New result from the MEG experiment at PSI

E. RIPICCINI on behalf of the MEG COLLABORATION

*Università di Roma "Sapienza" e INFN, Sezione di Roma
Piazzale A. Moro, 00185 Roma, Italy*

ricevuto l'1 Ottobre 2013

Summary. — The analysis of a combined data set, corresponding to 3.6×10^{14} stopped muons on target, in the search for the lepton flavor violating decay $\mu^+ \rightarrow e^+\gamma$ is presented. The data collected by the MEG experiment at the Paul Scherrer Institut show no excess of events compared to background expectations and thus yield a new upper limit on the branching ratio of this decay of 5.7×10^{-13} @ 90% CL (Adam J. *et al.*, *Phys. Rev. Lett.*, **110** (2013) 201801). This represents a four times more stringent limit than the previous world limit set by MEG.

PACS 13.35.Bv – Decays of muons.

PACS 14.60.Ef – Muons.

PACS 14.60.-z – Leptons.

1. – Introduction

The $\mu^+ \rightarrow e^+\gamma$ decay violates the lepton flavor conservation and it is then strongly suppressed in the Standard Model in the extension to massive neutrino [1], providing a sensitivity on the Branching Ratio experimentally unattainable ($\mathcal{O}(10^{-53})$). Most of the models beyond the Standard Model [2-5] allow the lepton flavor violation with a branching ratio for the $\mu^+ \rightarrow e^+\gamma$ decay much larger ($\mathcal{O}(10^{-13})$). The research of this channel represents a very good probe for models Beyond the Standard Model (BSM) validation, particularly if we take into account the recent measurement of θ_{13} at the reactors [6-8] and at accelerators [9]. Moreover a limit on the $BR(\mu^+ \rightarrow e^+\gamma)$ provides constraints on the parameters space of these models, complementary to those obtainable at high energy colliders.

The result shown in this paper was set using the data collected in 2009-2010-2011. An updated analysis for 2009 and 2010 with respect to the one presented in [10] is also shown.

The $\mu^+ \rightarrow e^+\gamma$ signature is given by back-to-back, monoenergetic, time coincident photon-positron pair. Each event is described by five observables: the photon and positron energy (E_γ, E_e), their relative angles ($\theta_{e\gamma}, \phi_{e\gamma}$) [11] and relative emission time ($t_{e\gamma}$).

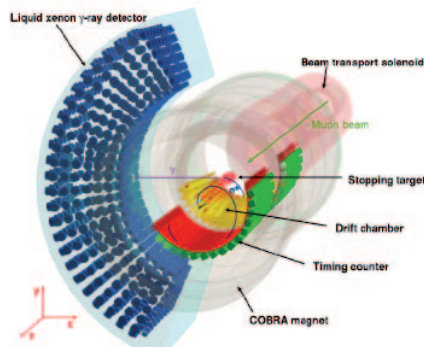


Fig. 1. – The MEG experiment.

Two are the main background sources: one coming from the radiative decay (RMD) when the two neutrinos take a small energy amount, one from the accidental (ACC) superposition of energetic positrons from the standard muon Michel decay with photons from RMD, positron-electron annihilation-in-flight or bremsstrahlung. The accidental background is the most important.

We use a maximum likelihood analysis technique described in detail in [10].

The MEG detector, in fig. 1, is comprised of a positron spectrometer formed by a set of drift chambers (DCH) and scintillation Timing Counter bars, located inside a superconducting solenoid, with a gradient magnetic field along the beam axis (1.27 T at the centre and 0.49 T at both ends), and a photon detector, located outside of the solenoid, made up of a homogeneous volume (900l) of liquid xenon, read by 846 UV-sensitive PhotoMultipliers. The MEG detector response, resolutions and stability are constantly monitored and calibrated with a multi-element calibration system [10, 12].

Concerning trigger and DAQ system, in 2011 the DAQ efficiency, being the product of DAQ live time fraction and trigger efficiency to select signal event, is at 96% level. It was 87% in 2010 and was improved thanks to a new multiple buffer read out scheme.

2. – Detector performances and analysis result

Concerning the positron reconstruction analysis some improvements have been introduced. Electromagnetic noise were reduced by introducing a new reconstruction algorithm based on the fast Fourier filtering techniques, providing a 10% improvement in angular resolution. The positron track is extracted by means of a Kalman filter track fitting technique [13, 14], completely revised for this analysis, to include a better model for the hits and track itself. It also provides per-track error, which is taken into account in the likelihood analysis. The overall improvement in the positron reconstruction with respect to the previous data analysis is visible in fig. 2 (left).

The energy resolution is evaluated by fitting the kinematic edge and it is well described by a sum of three Gaussian curves with a resolution of $\sigma_{E_e} = 305$ keV for the core (85%) component. The positron angular resolutions are measured by using the double turn method (two turns of the same track are treated as they were a single turn. The resolutions are evaluated in the point where the second turn starts), and they are respectively $\sigma_{\theta_e} = 10.6(10.6)$ mrad [15] and $\sigma_{\phi_e} = 7.5(7.0)$ mrad. The decay vertex coordinates and

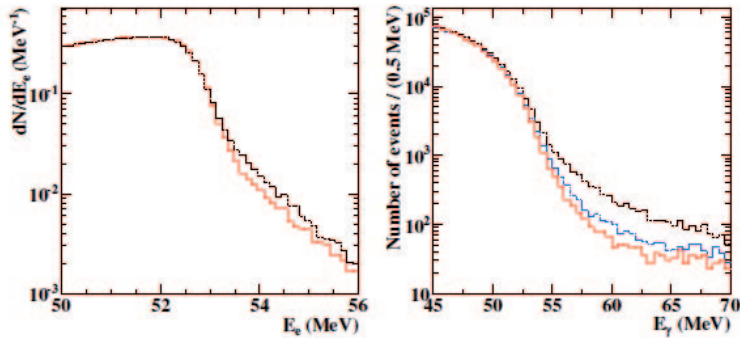


Fig. 2. – On the left the positron energy spectrum obtained with old analysis (black line), compared to the one obtained with the new analysis. The same configuration is shown for the photon on the left with the addition with the spectrum without pile-up rejection (blue line).

the positron direction at the vertex are determined by projecting the reconstructed track back to the target. The resolution on the decay vertex coordinates are also determined by the two turn method and are described by a Gaussian curve with $\sigma_z = 1.9(1.5)$ mm and, in the vertical direction, by the sum of two Gaussian curves with $\sigma_y = 1.3(1.2)$ mm for the core component (85%).

The xenon liquid calorimeter provides the energy, the time and the position of the first interaction of the photon. The direction of the photon is defined by the line connecting the decay vertex to the conversion point in the calorimeter. An important issue in the photon analysis is to identify and unfold photon pile-up events, since, with a beam rate of 3×10^7 mu/s, the 15% of triggered photons are affected by pile-up. For the previous analysis pile-up events were identified topologically by the pattern of PMT light distribution in both the inner and the outer LXe faces and temporally by the leading edge time distribution in the time reconstruction, without using any information from the waveform. In addition to this method, a new algorithm was developed, which analyzes waveforms after summing up all channels. The pile-up identification and rejection is based on a template fit. The resulting integrated charge is lower with respect to the one obtained with the old method, as a consequence the photon energy spectrum has reduced tail fig. 2 (right). The efficiency of the photon reconstruction is also improved from 56% to 67%.

Time and energy resolution are evaluated using back to back photons coming from the π^0 decay. The LXe timing resolution is $\sigma_{t_\gamma} = 67$ ps, while the position-dependent energy resolution is 1.7(1.9)% and 2.4(2.4)% from the radial depths larger and smaller than 2 cm respectively. These position-dependent energy resolutions are incorporated into the likelihood analysis.

By combining photon and positron resolutions, relative resolutions ($\theta_{e\gamma}, \phi_{e\gamma}$) are obtained. The results are $\sigma_{\theta_{e\gamma}} = 16.2(15.7)$ mrad and $\sigma_{\phi_{e\gamma}} = 8.9(9.0)$ mrad. The relative time $t_{e\gamma}$ is derived from the time measurements, one in the LXe detector and the other in the Timing Counter, after correcting for the length of the track given by the track fit. The $t_{e\gamma}$ resolution is $\sigma_{t_{e\gamma}} = 127(135)$ ps and it is evaluated from the RMD peak observed in E_γ sideband ($E_\gamma < 48$ MeV, $E_\gamma > 58$ MeV). The Background PDFs are evaluated in the blinding $t_{e\gamma}$ and E_γ regions, respectively $|t_{e\gamma}| < 1$ ns and 48 MeV $< E_\gamma < 58$ MeV.

TABLE I. – *Best fit and sensitivity.*

Dataset	$BR_{\text{fit}} \times 10^{12}$	$BR_{90} \times 10^{12}$	Sensitivity $\times 10^{12}$
2009+2010	0.17	1.7	1.3
2011	-0.35	0.67	1.1
2009+2010+2011	-0.06	0.57	0.77

A maximum likelihood fit is performed in order to extract the number of background events in the analysis region defined by $48 \text{ MeV} < E_\gamma < 58 \text{ MeV}$, $50 \text{ MeV} < E_e < 56 \text{ MeV}$, $|t_{e\gamma}| < 0.7 \text{ ns}$, $|\theta_{e\gamma}| < 50 \text{ mrad}$ and $|\phi_{e\gamma}| < 50 \text{ mrad}$. The definition of the likelihood function is described in detail in [10]. As mentioned before in the new analysis a per-event error matrix, estimated with the new Kalman filter, has been introduced in the PDFs. The confidence interval for the number of signal events is calculated by a frequentist method with profile likelihood-ratio ordering [10,16,17], where the numbers of RMD and ACC events are treated as nuisance parameters.

In order to convert the number of signal events into a branching ratio, two independent normalization methods are used: either counting the number of Michel positrons selected with a dedicated trigger or the number of RMD events observed in the muon data. Their combination leads to a 4% in the branching ratio uncertainty.

Concerning systematic uncertainties of PDFs parameters and normalization, they are taken into account in the calculation of the confidence interval by fluctuating the PDFs parameters by the amount of the uncertainties. The systematic uncertainties contribution to the branching ratio is at 1% level. In order to estimate the sensitivity, a number of pseudo-experiments are performed according to the PDFs in the null-hypothesis, with the values of RMD and ACC estimated in the sidebands. The sensitivity is the median of the distribution of the branching ratio upper limit at 90% C.L. In table I the summary of the observed upper limits are reported. The profile likelihood as a function of the branching ratio is shown in fig. 3. The upper limit, obtained combining 2009-2011 data taken, is 5.7×10^{-13} @ 90% CL. A summary of the previous upper limits is reported in table I. In

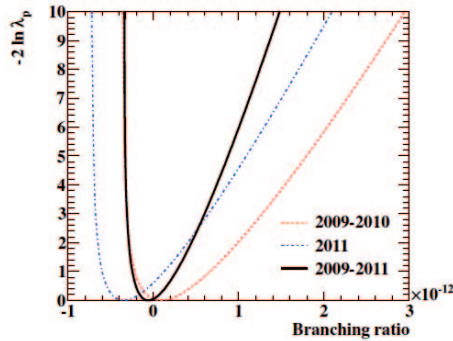


Fig. 3. – Observed profile likelihood ratios λ_p as a function of the branching ratio for the 2009-2010 combined data, the 2011 data alone and the combined 2009-2011 data sample.

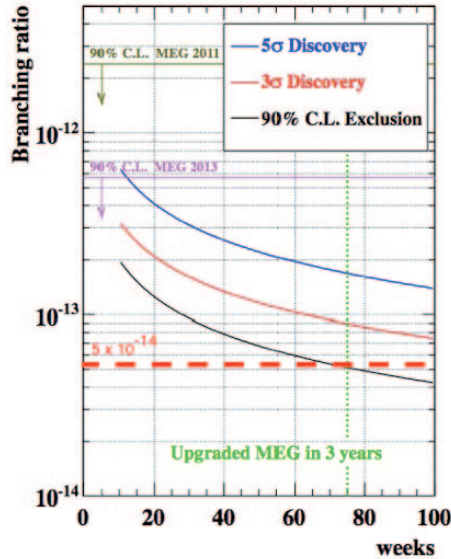


Fig. 4. – Branching ratio as a function of the data taken weeks with the upgraded detector. After 3 years a sensitivity of 5×10^{-14} is expected.

order to have a crosscheck of the results, a maximum likelihood fit is repeated without the constrain on the number of background events. We obtain $N_{RMD} = 163.1 \pm 31.5$ and $N_{ACC} = 2411.1 \pm 56.9$, in good agreement with the expectation value estimated from the sidebands: $\langle N_{RMD} \rangle = 169.3 \pm 17.0$ and $\langle N_{ACC} \rangle = 2415.0 \pm 25.0$. Concerning 2009-2010 analysis, we compared the result obtained with the new analysis to the previous one based on the old analysis, generating simulated experiments. We found that the probability to found a result equal to or larger than the old one is 31%.

3. – Conclusions

In conclusion the MEG experiment established the most stringent upper limit on the branching ratio of the $\mu^+ \rightarrow e^+ \gamma$ decay. We have to analyze more data taken during 2012, while the 2013 run is now on going. The final number of muon stopped on target is expected to be double than the one analyzed so far. With the whole data set (2009-2013) a sensitivity of $5 \cdot 10^{-13}$ is expected. At this point the limit decreases as the inverse of \sqrt{t} , where t is the data taking time and the background becomes predominant in the signal region. Therefore in order to exploit sensitivity at least an order of magnitude lower, a new upgraded MEG experiment is required. An upgrade program was approved in January 2013. The main features of the upgrade are: a higher beam sensitivity, a single volume drift chamber with stereo angle wires configuration, a scintillator tile timing counter with SiPM readout, substitution of the PMTs in the inner face of the calorimeter with SiPM and a larger liquid Xenon fiducial volume. The expected sensitivity with 3 year run with the new detector is 5×10^{-14} as shown in fig. 4. There is also a possibility to install an active target which can provide the decay vertex position improving resolutions for the positron and the normalization factor. Further detail concerning the upgrade can be found in [18].

REFERENCES

- [1] PETCOV S. T., *Sov. J. Nucl. Phys.*, **25** (1977) 340.
- [2] BARBIERI R., HALL L. and STRUMIA A., *Nucl. Phys. B*, **445** (1995) 219.
- [3] HISANO J., NOMURA D. and YANAGIDA T., *Phys. Lett. B*, **437** (1998) 351.
- [4] RAIDAL M. *et al.*, *Eur. Phys. J. C*, **57** (2008) 13.
- [5] BLANKENBURG G. *et al.*, *Eur. Phys. J. C*, **72** (2012) 2126.
- [6] AN F. P. *et al.*, *Phys. Rev. Lett.*, **108** (2012) 171803.
- [7] AHN J. K. *et al.*, *Phys. Rev. Lett.*, **108** (2012) 191802.
- [8] ABE Y. *et al.*, arXiv:1301.2948 [hep-ex].
- [9] ABE K. *et al.*, *Phys. Rev. Lett.*, **107** (2011) 041801.
- [10] ADAM J. *et al.*, *Phys. Rev. Lett.*, **107** (2011) 171801.
- [11] $\theta_{e\gamma} = (\pi - \theta_e) - \theta_\gamma$ and $\phi_{e\gamma} = (\pi + \phi_e) - \phi_\gamma$, θ and ϕ being the polar angle and the azimuthal angle, respectively, taking the z -axis as the beam-axis.
- [12] ADAM J. *et al.*, *Eur. Phys. J. C*, **73** (2013) 2365.
- [13] CMS COLLABORATION, *JINST*, **5** (2010) T03009.
- [14] BILLOIR P., *Nucl. Instrum. Methods A*, **225** (1984) 352.
- [15] From here on we will quote in parentheses the value in the 2009–2010 data when different from that in 2011.
- [16] BERINGER J. *et al.* (PARTICLE DATA GROUP), *Phys. Rev. D*, **86** (2012) 010001.
- [17] FELDMAN G. J. and COUSINS R. D., *Phys. Rev. D*, **57** (1998) 3873.
- [18] BALDINI A. M. *et al.*, arXiv:1301.7225 [physics.ins-det].